Sonophotocatalytic mineralization of Norflurazon in aqueous environment

Article *in* Chemosphere · March 2016

DOI: 10.1016/j.chemosphere.2015.12.011

7 authors, including:

Panneerselvam Sathishkumar
University of Concepción
38 PUBLICATIONS **734** CITATIONS
SEE PROFILE

Oscar Rozas
University of Concepción
8 PUBLICATIONS **96** CITATIONS
SEE PROFILE

Miguel Ángel Gracia Pinilla
Autonomous University of Nuevo León
48 PUBLICATIONS **264** CITATIONS
SEE PROFILE

Anandan Sambandam
National Institute of Technology Tiruchirappalli
198 PUBLICATIONS **2,788** CITATIONS
SEE PROFILE

Chemosphere 146 (2016) 216–225

Contents lists available at ScienceDirect

Chemosphere

journal homepage: www.elsevier.com/locate/chemosphere

Sonophotocatalytic mineralization of Norflurazon in aqueous environment

Panneerselvam Sathishkumar [a, b, *], Ramalinga Viswanathan Mangalaraja [a, **], Oscar Rozas [c], Carola Vergara [d], Héctor D. Mansilla [c], M.A. Gracia-Pinilla [e, f], Sambandam Anandan [g]

[a] Advanced Ceramics and Nanotechnology Laboratory, Department of Materials Engineering, Faculty of Engineering, University of Concepcion, Concepcion 407-0409, Chile
[b] Department of Chemistry, Periyar Maniammai University, Vallam, Thanjavur 613403, Tamil Nadu, India
[c] Faculty of Chemical Sciences, University of Concepcion, PO Box 160-C, Correo 3, Concepcion, Chile
[d] Instrumental Analysis Department, Faculty of Pharmacy, University of Concepción, PO Box 160-C, Correo 3, Concepción, Chile
[e] Universidad Autónoma de Nuevo León, Facultad de Ciencias Físico-Matemáticas, Av. Universidad, Cd. Universitaria, San Nicolás de los Garza, N.L., Mexico
[f] Universidad Autónoma de Nuevo León, Centro de Investigación e Innovación en Desarrollo de Ingeniería y Tecnología, Avenida Alianza 101 Sur PIIT Monterrey, Apodaca, N.L. 66600, Mexico
[g] Nanomaterials and Solar Energy Conversion Lab, Department of Chemistry, National Institute of Technology, Trichy 620 015, India

HIGHLIGHTS

- 42 kHz ultrasound assisted Au and Au–ZnO nanocatalysts were synthesized.
- Photocatalytic, sonocatalytic and sonophotocatalytic mineralization was studied.
- Intermediates produced from the Norflurazon were analyzed by ESI-MS analysis.

GRAPHICAL ABSTRACT

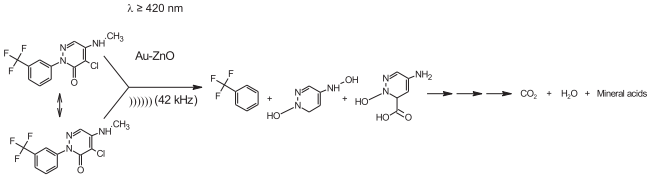

ARTICLE INFO

Article history:
Received 12 March 2015
Received in revised form
19 October 2015
Accepted 6 December 2015
Available online xxx

Handling Editor: Jun Huang

Keywords:
Norflurazon
Mineralization
Sonophotocatalysis
Visible light
HPLC and LC-MS analyses

ABSTRACT

Norflurazon (4-chloro-5-(methylamino)-2-[3-(trifluoromethyl)phenyl]pyridazin-3(2H)-one; $C_{12}H_9ClF_3N_3O$) is an excellent weed controlling agent being practiced in the agricultural lands. The excessive addition or the undissolved Norflurazon (maximum solubility 28 mg/L at 25 °C) enters into the aquatic environment and causes the adverse effects associated with its high concentration. To avoid the perilous effects, visible light assisted photocatalysis set-up coupled with the 42 kHz ultrasound producing bath type sonicator is used to completely mineralize the Norflurazon. TiO_2, ZnO and gold loaded zinc oxide nanocatalysts were utilized to study the mineralization of Norflurazon. Au–ZnO shows the greater efficiency for the sonophotocatalytic removal of Norflurazon among the various nanocatalysts employed to study the mineralization. The order of Norflurazon mineralization was sonophotocatalysis > sonocatalysis > photocatalysis. The additive effect was achieved for the sonophotocatalytic degradation. The high performance liquid chromatography (HPLC) and liquid chromatography-mass spectrometric (LCMS) analyses were employed to identify the various intermediates produced during the mineralization. The identification of four pseudo molecular ions and various intermediates using the LCMS analysis evidently suggests the

* Corresponding author. Advanced Ceramics and Nanotechnology Laboratory, Department of Materials Engineering, Faculty of Engineering, University of Concepcion, Concepcion 407-0409, Chile.
** Corresponding author.
E-mail addresses: sathish_panner2001@yahoo.com (P. Sathishkumar), mangal@udec.cl (R.V. Mangalaraja).

http://dx.doi.org/10.1016/j.chemosphere.2015.12.011

sonophotocatalytic degradation was preceded in various decay pathways. A suitable mechanism has been proposed for the sonophotocatalytic mineralization of Norflurazon.

1. Introduction

The quantity of pesticide usage in the agricultural land has been considerably increased due to the worldwide modernization of the agriculture. The usage of pesticides throughout the world was approximately calculated as 2.5 million tons and the need of pesticide was estimated to increase in the forthcoming years (Arias-Estevez et al., 2008; Pimentel, 1995). The herbicides alone occupy nearly 50% of the various categories of pesticides being practiced in the agricultural lands (Drogui and Lafrance, 2012). Among the various herbicides, Norflurazon is a bleaching, pre-emergence and selective herbicide used in the agriculture lands since 1974 (Ahrens, 1994). Norflurazon is a long-standing contaminant in the soil, it will not easily undergo mineralization and gradually be desorbed which depends on the agricultural environmental conditions (Morillo et al., 2004). A very low quantity of herbicide is practically involved in the weed control when Norflurazon is applied in the agricultural lands. Major quantity enters into the environment which causes the soil and aquatic pollution. The custom of Norflurazon leads to detect the herbicide in the water resources more frequently which continuously alarming the negative impacts associated with the herbicide usage (Wilson and Boman, 2011). In addition to that the increased concentration of Norflurazon (>16 mg/L) in the agricultural land inhibits the carotene synthesis in plants, which destroys the chlorophyll (Wilkinson, 1985; Bramley, 1993). Therefore it needs to be completely mineralized to avoid the hazardous effects engendered by the Norflurazon at its high concentrations.

On the other hand, zinc oxide (ZnO) provokes various interesting nanostructures during its synthesis. The properties like large direct band gap ($E_g = 3.37$ eV), excitation binding energy (60 MeV), near-UV emission, transparent conductivity and piezoelectricity which make ZnO as a unique promising nanomaterial for the energy and environmental applications (Huang et al., 2011; Ozgur, 2010; Umar et al., 2012; Wang et al., 2004). The photocatalysis was found to be very interesting among the various applications of ZnO and it can be extensively applied for the degradation of various environmental contaminants. In certain occasions, ZnO has revealed greater photocatalytic efficiency than the TiO_2 (Li et al., 2010; Sakthivel et al., 2003). However the quantum yield achieved for the visible light assisted ZnO photocatalysis needs to be improved (Chen et al., 2014; Sathishkumar et al., 2009; Kim and Yong, 2012). The appropriate technique to enhance the photocatalytic activity of ZnO is to decrease the recombination of electronic charges (holes and electrons) which are instigated during the photocatalysis. Since the deferred recombination of electronic charges enhances the active radicals produced from the photocatalytic microenvironment. The loading of noble metal nanoparticles (Au, Ag and Pt) significantly increases the optical as well as catalytic properties of the resulting ZnO nanocatalysts (Subramanian et al., 2003; Lee et al., 2008; Wang et al., 2003).

Among the various metal nanoparticles, gold nanoparticles have proven the following exceptional properties: (i) The surface plasmon resonance (SPR) was found to be improved the local electric field when the gold nanoparticles are in contact with the semiconductor nanocatalysts. Thus accelerates the generation of electronic charges when the nanocatalysts experience the band gap excitation (Subramanian et al., 2003); (ii) The gold nanoparticle acts as a sink for the electronic charges produced at the interface of the metal-semiconductor (Kamat and Meisel, 2002); (iii) The difference in the work function of Au ($\varnothing_m = 5.1$ eV) and ZnO ($\varnothing_s = 4.3$ eV) leads to generate the schottky barrier which further facilitates the transport of electronic charges (Kamat and Meisel, 2002; Wood et al., 2001). Hence, the gold nanoparticles loaded semiconductor nanocatalysts was found to be very efficient for the degradation of various environmental contaminants. In the present work, a low frequency ultrasound (42 kHz) was utilized for the preparation of Au–ZnO nanocatalysts. The sonocatalytic, photocatalytic and sonophotocatalytic efficiencies were investigated by studying the mineralization of Norflurazon in the presence of TiO_2, ZnO and gold loaded ZnO nanocatalysts. The combination of bath type sonicator (42 kHz) with the visible light assisted photocatalysis technique is expected to enhance the efficiency of the mineralization when compared with the individual advanced oxidation processes.

2. Experimental

2.1. Materials and methods

Norflurazon ($C_{12}H_9ClF_3N_3O$), Zinc dioxide and chloroauric acid trihydrate ($HAuCl_4 \cdot 3H_2O$) were purchased from Sigma-Aldrich and used without further purification. Unless otherwise specified, all the reagents used were of analytical grade and the solutions were prepared using Milli-Q water. Surface morphology and microstructure of the nanocatalysts were analyzed by high resolution transmission electron microscopy (HRTEM, FEI TITAN G2 80-300) operated at 300 KeV and field emission scanning electron microscopy (FEI-Nova nanosem 200). The particle size of the synthesized nanoparticles was calculated from the X-ray diffraction data (Philips PW1710 diffractometer, CuK_α radiation, Holland) using Scherrer equation. Raman spectra were recorded using a Dilor LabRam-1B spectrometer, operating at a resolution of 1 cm^{-1}. Diffuse reflectance UV–vis spectra of the nanocatalysts were recorded using a Shimadzu 2550 spectrophotometer equipped with an integrating sphere accessory employing $BaSO_4$ as reference material.

The kinetics of Norflurazon degradation was followed using a HPLC (Perkin Elmer) analyzer equipped with a PDA detector (model Flexar). C18 column (150 × 4.6 mm, 2.6 μm, Kinetex, Phenomenex, USA) was employed for the analysis. The UV detection was operated at 310 nm, and the mobile phase constituted by acetonitrile (50%) and water (50%). The injection volume was 20 μL and the flow rate was 0.5 mL/min. The retention time for Norflurazon was 7 min under these HPLC conditions. Calibration curve for Norflurazon was constructed using the peak areas of the standard samples under the same conditions as that of the experimental samples. A fresh stock solution of Norflurazon was prepared before the experiments. Norflurazon calibration curve was made for concentrations between 0.01 and 28 mg/L with a correlation coefficient of $R^2 = 0.9998$. The total organic carbon (TOC) for all the samples was analyzed by direct injection of the filtered sample solutions into a TOC analyzer (Vario TOC cube, Cientec Instrumentos, South America). Prior to the analysis, the instrument was calibrated with

potassium hydrogen phthalate. TOC_0 is the TOC measured after the equilibrium adsorption of the dye on the nanocatalysts surface and TOC obtained at various irradiation times is denoted as TOC_t.

The LC-MS analysis of Norflurazon was performed in a Nexera UHPLC System (Shimadzu, Japan) equipped with a DAD detector and coupled with a 3200 QTRAP Mass Spectrometer (ABsciex, USA, MA). Instrument control and data collection system were carried out using Analyst 1.5.2 software (ABsciex, USA, MA). The chromatographic separation was achieved on C18 column (150 × 4.6 mm, 2.6 μm, Kinetex, Phenomenex, USA). Mobile phase was constituted by acetonitrile (60%) and formic acid 0.1% in water (40%) at a flow rate of 0.5 mL min^{-1} in an isocratic mode. The detection wavelength was set at 300 nm and the injection volume was 10 μL. The MS/MS detection was carried out under the following conditions: electrospray positive ionization mode, 10 V of collision energy, 3000 V of ionization voltage and capillary temperature at 300 °C. Nitrogen was used as nebulizing (30 psi) and drying (10 psi) gas.

2.2. Preparation of gold and gold loaded ZnO nanocatalysts

The ultrasound assisted reduction of Au^{3+} to Au^0 was performed as follows: The gold precursor solution (5.25×10^{-4} M) was prepared with 0.1 M of isopropanol and 0.1 wt% of polyethylene glycol under the vigorous stirring. The precursor was irradiated by 42 kHz ultrasound up to 30 min. The samples were withdrawn at regular intervals during the irradiation for the UV–vis spectroscopic analysis (Fig. 1(a)). The gold precursor solution (Au^{3+}) produced its characteristic yellow color during preparation, which later turned to bluish violet color (Au^0) after the completion of ultrasound irradiation. Presumed here in 30 min that all Au^{3+} was converted to Au^0. Nevertheless the absence of Au^{3+} characteristic peak during the UV–vis spectroscopic analysis confirms that the entire precursor was converted to gold nanoparticles (Wei et al., 2013; Mizukoshi et al., 2005). The obtained gold nanoparticles were characterized using various analytical tools.

The gold precursor solution (5.25×10^{-4} M) in 0.1 M of isopropanol solution was stirred vigorously for 15 min and subsequently the zinc oxide (1 g) was added. The suspension was irradiated till the change of color of the suspension from yellow to bluish violet. It was assumed that the above procedure yielded a gold loading of ~1 mol% on ZnO. The nanocatalysts were gathered by filtration using 0.45 μm nylon membrane. The solids were dried at 110 °C in a hot air-oven for 12 h followed by the calcination at 550 °C for 5 h in order to get pure nanocatalysts. Similarly the bare ZnO was treated using the same methodology and calcinated at 550 °C for comparison.

2.3. Photocatalysis and sonophotocatalysis

The stock solution of Norflurazon was freshly prepared by dissolving appropriate amount of Norflurazon in Milli-Q water. The concentration of Norflurazon for all the degradation studies was fixed to 28 mg/L which provided the maximum solubility in water at 25 °C (Wilson and Boman, 2011). The stock solutions were filtered using a 0.2 μm Polytetrafluoroethylene syringe filter (PTFE, Cole-Parmer, USA) before all the experiments. The degradation of Norflurazon was studied under ambient atmospheric conditions and at natural solution pH. In order to ensure the adsorption/desorption equilibrium, the Norflurazon/nanocatalyst slurry was stirred for 45 min in dark condition prior to irradiation. After that, the lamp and/or the sonicator was turned on to consider as "time zero" to follow the kinetics of degradation. The photocatalytic studies were performed using a light source (Cole-Parmer, USA) illuminating spectral range ≥ 420 nm with the intensity of incident irradiation ≥ 100,000 ± 100 Lux measured by Lux meter (Cole-Parmer, USA). All the sonochemical reactions in this study were carried out by using a commercially available sonicator (8890, Cole-Parmer, USA) producing 42 kHz ultrasound waves. The experimental setup and conditions used for photolysis, sonolysis, and sonophotolysis were identical (Sathish Kumar et al., 2010). The Norflurazon was irradiated with visible light, nanocatalysts (dark) and ultrasound separately to study the effect of photolysis and sonolysis. No apparent rate of Norflurazon degradation was observed from the photolysis and in the presence of nanocatalysts (dark). The significant rate of Norflurazon degradation was achieved during the sonolysis which presented in Table 1. The apparent kinetics of disappearance of Norflurazon was determined by following its concentration using HPLC analysis. Prior to the analysis, the nanocatalysts were separated from the suspension by using a 0.2 μm PTFE filter.

3. Results and discussion

3.1. Characterization of gold and gold loaded ZnO nanocatalysts

The characteristic changes observed during the transformation of Au^{3+} to Au^0 was monitored using a UV–vis spectrophotometer and the observed results are shown in Fig. 1(a). The formation of gold nanoparticles instigates after 3 min of irradiation of the precursor solution and the completion of gold nanoparticles formation was achieved within 30 min. The extended ultrasound irradiation (>30 min) leads to initiate the aggregation (Zhu et al., 2009). The TEM analysis revealed the gold nanoparticles of size ranging from 2 to 5 nm as shown in Fig. 1(b). The lattice fringe distance calculated from Fig. 1(b) is 0.23 nm which is the clear indication for the formation of Au (1 1 1) crystal plane during the ultrasound irradiation. The FESEM (Fig. 1(c)) and TEM (Fig. 1(d)) analyses of the bare ZnO reveal various morphology of nanostructure. However, the sonochemically treated ZnO exhibits nanorod structure as preponderance of evidence from the high angle annular dark field (HAADF) scanning transmission electron microscopic (STEM) analysis (Fig. 1(e)). The EDX analysis of bare ZnO is shown in Fig. 1(f).

The TEM analysis of the gold nanoparticles loaded ZnO displays various nanostructures and is shown in Fig. 2. The Au loading reduces the length of the nanorods but the thickness gets increased. The observed transformation evidently suggests that the crystallinity of the ZnO gets altered nonetheless the crystal structure. Besides, the decorated gold nanoparticles can be easily seen at the surface of the Au–ZnO (Fig. 2(c)–(e)). The calculated value of average size of the deposited gold nanoparticles is ~8 nm. The average particle size of the gold nanoparticles decorated at the surface of ZnO gets increased when compared with the particle size achieved for the bare Au nanoparticles since the addition of polyethylene glycol during the synthesis directly influences on the particle size (Zhu et al., 2009). The EDX analysis of Au–ZnO (Fig. 2(f)) confirms the elemental composition of the synthesized nanocatalysts.

The XRD patterns of the ZnO and Au–ZnO are shown in Fig. 3. The attributed diffraction peaks correspond to the wurtzite structure (JCPDS No. 36-1451), which designate that the crystal structure of ZnO is not changed after the modification with the gold nanoparticles however the intensity of wurtzite peaks gets reduced. In addition to that a weak diffraction peak ascribed to Au (1 1 1) in the XRD pattern of Au–ZnO (Insert Fig. 3) demonstrates the low quantity loading of gold nanoparticles (1 mol%). The XRD analysis confirms that the gold nanoparticles exist as their cubic (fcc) structure and the ZnO exists as its hexagonal (wurtzite) structure in the Au–ZnO nanocatalysts. However no other diffraction peaks belonging to the impurities like Au_2O_3 were observed in the XRD

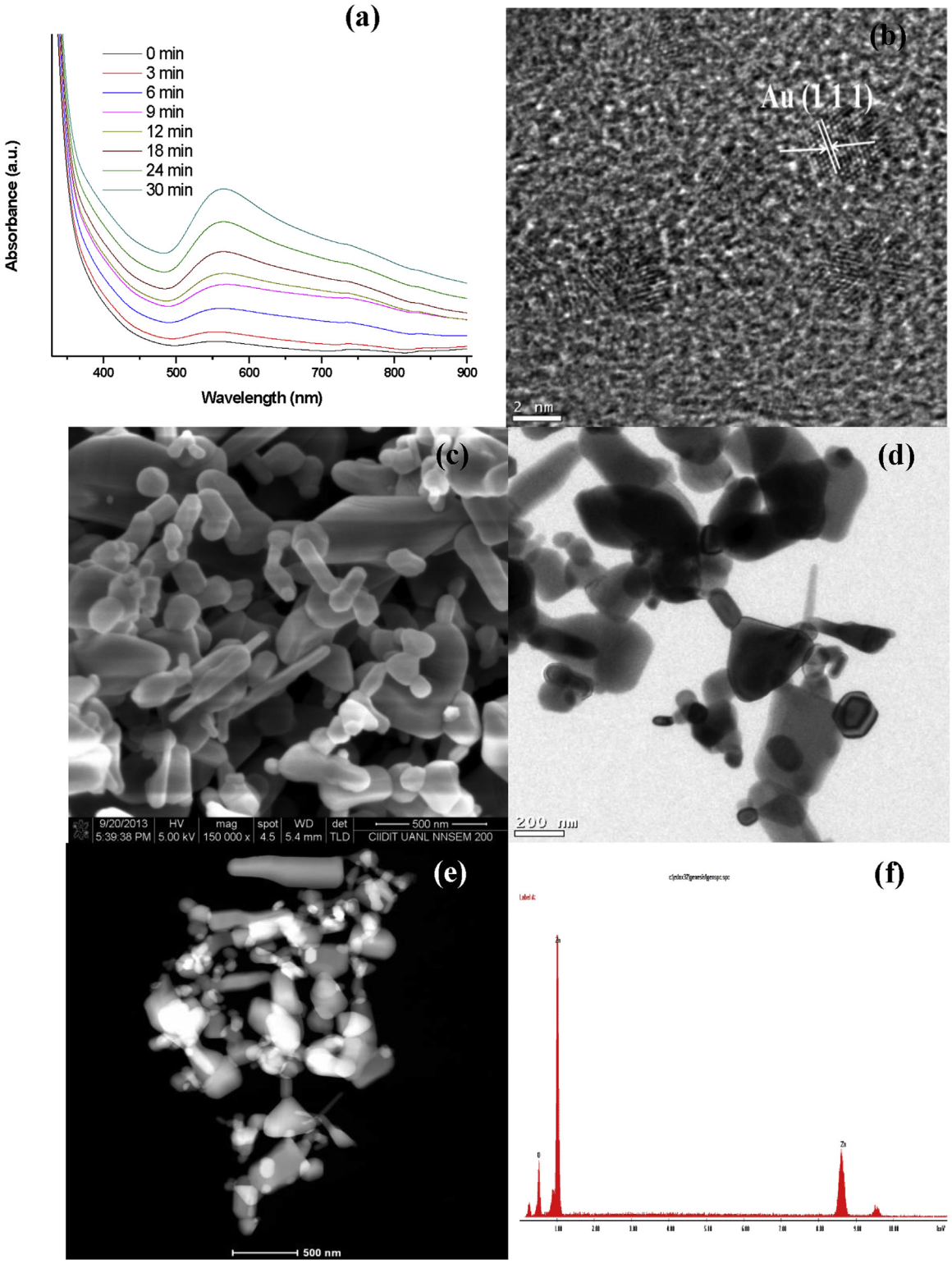

Fig. 1. (a) UV–vis absorption spectra of sonochemically reduced Au nanoparticles at various time intervals; (b) Representative HRTEM image of Au nanoparticles; Representative (c) FESEM; (d) TEM and (e) HAADF images and (f) EDX analysis of ZnO.

pattern. The room temperature Raman spectra observed for the ZnO and Au–ZnO nanocatalysts are presented in Fig. 4. The observed Raman spectra are consisting of several bands that correspond to the Raman-active phonon modes of wurtzite ZnO nanocatalysts with C_{6V} symmetry. The intensive peak observed at 439 cm^{-1} corresponds to the E_2 mode of ZnO which is a characteristic Raman-active mode for the hexagonal ZnO. Similarly the weak peaks observed at 333, 385, and 415 cm^{-1} can be assigned to the E_2 (high) – E_1, A_1 and E_1 Raman active modes of ZnO (Wang et al., 2008). The Raman peak emanated at 581 cm^{-1} becomes

Table 1
Degradation rate constant obtained for different processes using [nanocatalyst] = 1 g/L and [Norflurazon] = 28 mg/L.

S. no	Process	Nanocatalyst	Rate, 10^{-4} s^{-1}
1.	Photocatalysis	TiO_2	0.49
		ZnO	0.62
		Au–ZnO	1.60
2.	Sonolysis	–	0.38
3.	Sonocatalysis	TiO_2	1.59
		ZnO	1.93
		Au–ZnO	2.92
4.	Sonophotocatalysis	TiO_2	1.74
		ZnO	2.45
		Au–ZnO	4.1

broadened and disordered since it is the mixture of two modes (A_1 and E_1) (Meng et al., 2012). The intensity of Raman active peaks gets decreased and broadened when the gold nanoparticles loaded into the ZnO which indicates that gold nanoparticles reside at the surface of ZnO. It can be concluded from the Raman analysis that 42 kHz of ultrasound irradiation kindled the adequate distribution of gold nanoparticles on the surface of the ZnO. The loading of gold nanoparticles into ZnO cannot make any significant changes in the crystal structure. It can also be evidenced from the XRD and TEM analyses. The bare gold nanoparticles have not shown any Raman active modes during the analysis.

The diffuse reflectance (DR) UV–vis spectral analysis of ZnO and Au–ZnO is shown in Fig. 5. The extreme absorption for the bare ZnO is ~390 nm which significantly indicates that the bare ZnO cannot

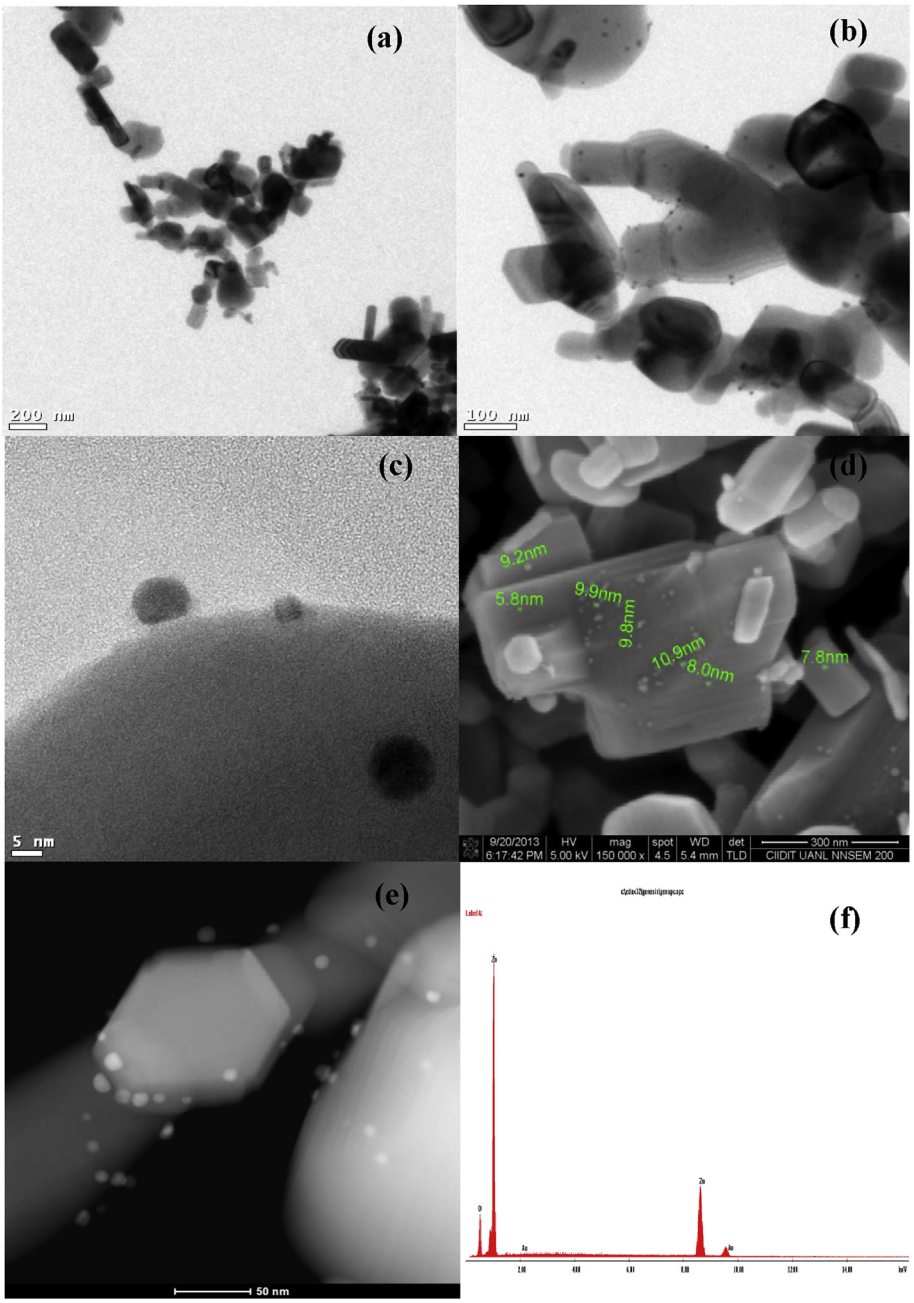

Fig. 2. TEM [(a) 200 nm; (b) 100 nm and (c) 5 nm], FESEM (d) and HAADF-STEM (e) images of Au–ZnO and (f) shows the corresponding EDX analysis of Au–ZnO nanocatalysts.

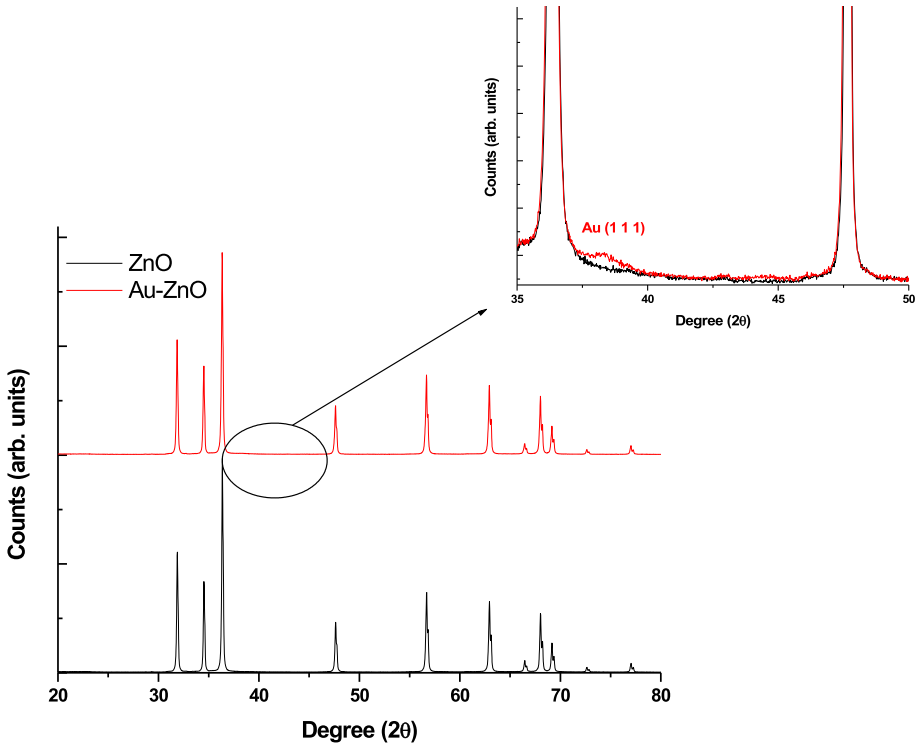

Fig. 3. X-ray diffraction analysis of ZnO and Au–ZnO nanocatalysts and the insert shows the expanded XRD region (2θ = 35–50).

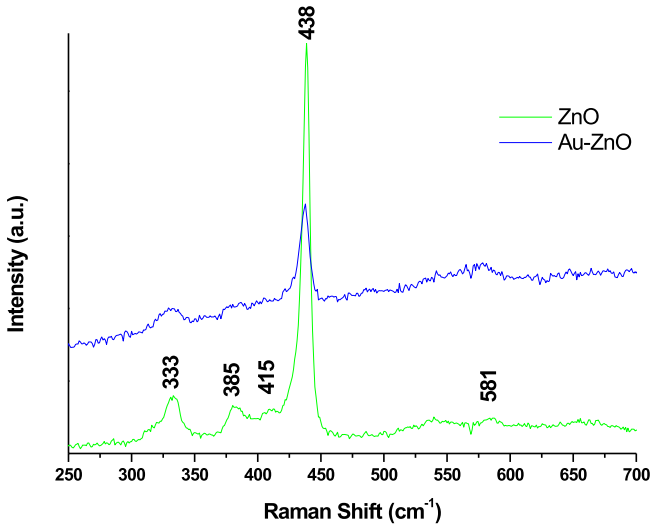

Fig. 4. Raman spectra of ZnO and Au–ZnO nanocatalysts.

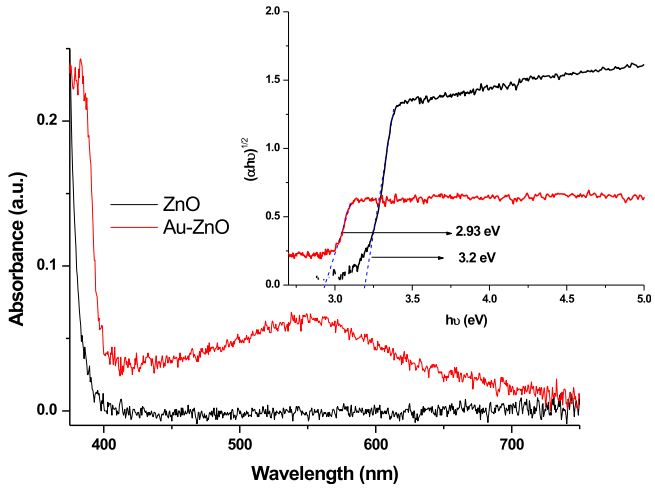

Fig. 5. Diffuse reflectance (DR)-Uv–Vis spectra of ZnO and Au–ZnO nanocatalysts and the insert shows the Tauc plot derived from the KubelkaMunk Function for ZnO and Au–ZnO.

be able to absorb the maximum portion of visible light. The absorption band edge of the gold loaded ZnO significantly shifted from 390 nm and the Au–ZnO nanocatalysts are expected to show the enhanced visible light assisted photocatalytic properties. The SPR peak observed at ~550 nm confirms that the visible light is adequate to generate the electronic charges during the irradiation. The Tauc plot derived from Kubelka Munk Function (inset of Fig. 5) shows that the optical band gaps are 3.2 eV and 2.93 eV for the bare ZnO and Au–ZnO respectively. The decreased band gap further enhances the possibilities of utilizing Au–ZnO as a visible light driven photocatalysts for the degradation of wide spectrum of organic contaminants.

3.2. Degradation of Norflurazon

The sonocatalytic, photocatalytic and sonophotocatalytic degradations of Norflurazon were evaluated in the presence and absence of ZnO, TiO_2 (Aeroxide® P25) and Au–ZnO nanocatalysts. The initial concentration of Norflurazon was fixed at its maximum solubility (28 mg/L) for all the degradation processes and the concentration of the nanocatalysts was varied from 0.2 to 3 g/L in order to optimize the appropriate dosage to achieve the maximum efficacy. The first order kinetics was observed for the Norflurazon degradation which can be evidenced from the straight line fit of $-\ln(C/C_0)$ vs time. A representative three dimensional HPLC

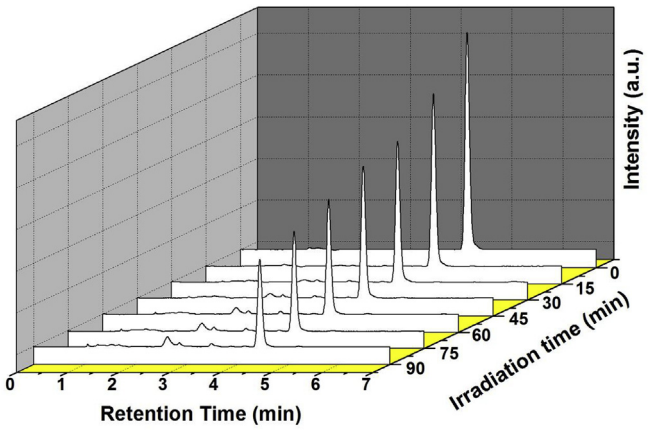

Fig. 6. 3-D plot showing the evolution of the HPLC chromatogram for the sonophotocatalytic degradation of Norflurazon at its optimized initial concentration 28 mg/L and [Au–ZnO] = 1.0 g/L.

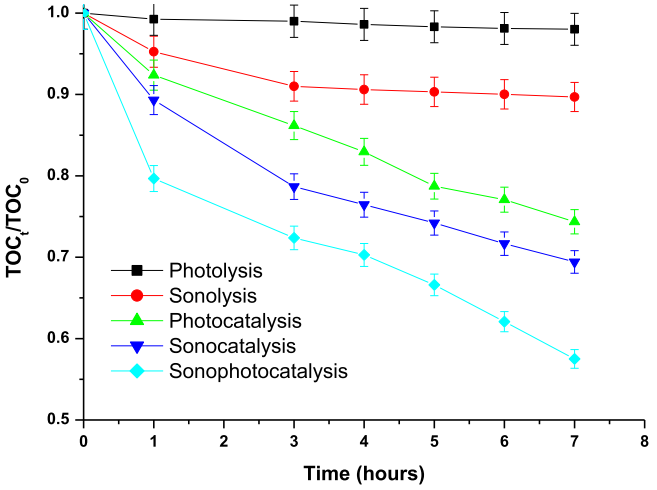

Fig. 8. Mineralization of Norflurazon (28 mg/L) during various advanced oxidation processes in the presence of Au–ZnO (1.0 g/L) nanophotocatalysts.

chromatogram obtained for the Norflurazon degradation at the optimized concentration ([Norflurazon] = 28 mg/L and [Au–ZnO] = 1 g/L) is shown in Fig. 6. The optimized concentration of the nanocatalysts provides an effective environment for the degradation process, which increases the interaction between effective radicals and Norflurazon (as well as its derivatives) during the degradation. The observed decrease in the Norflurazon concentration (Retention time (RT) = 4.5 min) clearly indicates the rapid degradation during the sonophotocatalysis (Fig. 6). The less-intensive peaks seemed at the RT from 2.25 to 4.25 min give the first notation about the intermediates produced from the Norflurazon and the intensity of the peaks get increased when the processing time progresses.

In order to understand the efficiency of the various advanced oxidation processes, a three dimensional HPLC chromatogram was observed for the photocatalytic, sonocatalytic and sonophotocatalytic degradation of Norflurazon and is presented in Fig. 7 before and after 90 min. The order of kinetics for the Norflurazon degradation was sonophotocatalysis > sonocatalysis > photocatalysis. The sonophotocatalytic and sonocatalytic degradation of Norflurazon show 4.5 and 2-fold enhanced rate of degradation when compared to the photocatalytic degradation. However, an additive effect of photocatalysis and sonocatalysis was observed for the sonophotocatalysis which can be evidenced from Fig. 7. In addition to that, the rate constants achieved during the sonolysis of Norflurazon was significantly lower than the rate constant observed for the photocatalysis (Table 1). The visible light assisted photocatalytic irradiation of Au–ZnO leads to initiate the electronic charges at the surface of nanocatalysts and thus enhances the number of active radicals produced at the photocatalytic microenvironment.

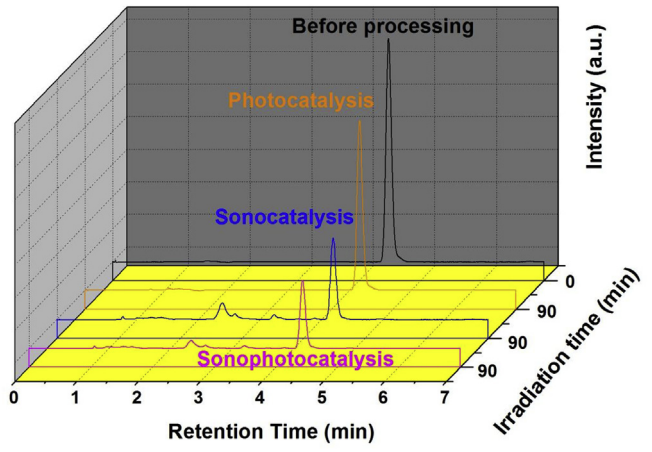

Fig. 7. 3-D plot showing the evolution of the HPLC chromatogram during the various advanced oxidation assisted degradation of Norflurazon at its optimized initial concentration 28 mg/L and [Au–ZnO] = 1.0 g/L.

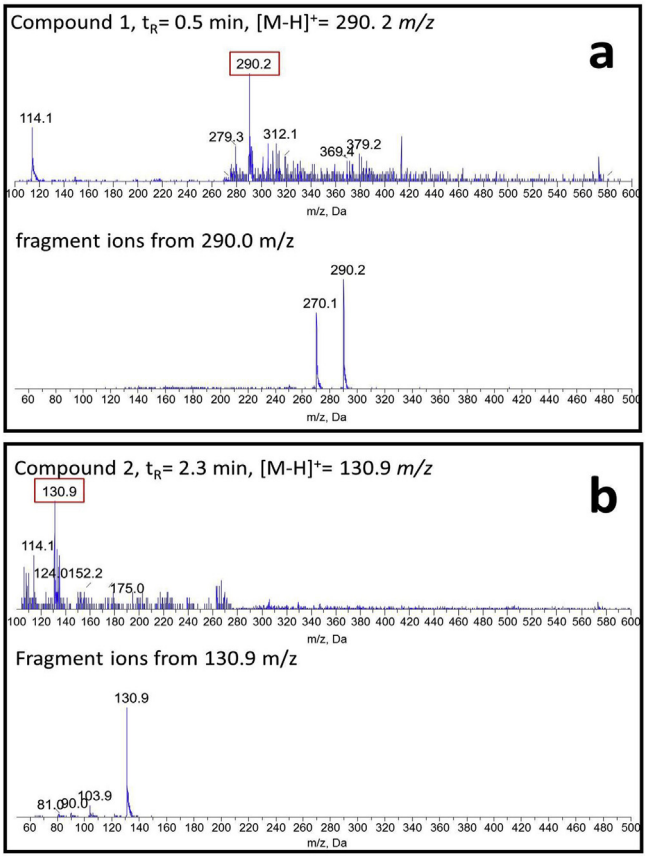

Fig. 9. HPLC-ESI-MS/MS chromatograms observed for the sonophotocatalytic mineralization of Norflurazon and its intermediates produced at (a) 30 min and (b) 120 min irradiation time.

Table 2
Spectral data of HPLC-ESI-MS/MS peak identification.

S. no	Compound	Peak	t_R (min)	Pseudo molecular ion [M − H] + (*m*/*z*)	Product ion (*m*/*z*)
1.	Desmethyl norflurazon	I	0.5	290.1	270.1
2.	4-(hydroxyamino) pyridazine	II	2.3	130.9	103.9, 90.0, 81.0
3.	Norflurazon	III	3.0	304.1	284.2, 264.2
4.	Norflurazon isomer	IV	3.5	304.1	284.0, 114.1

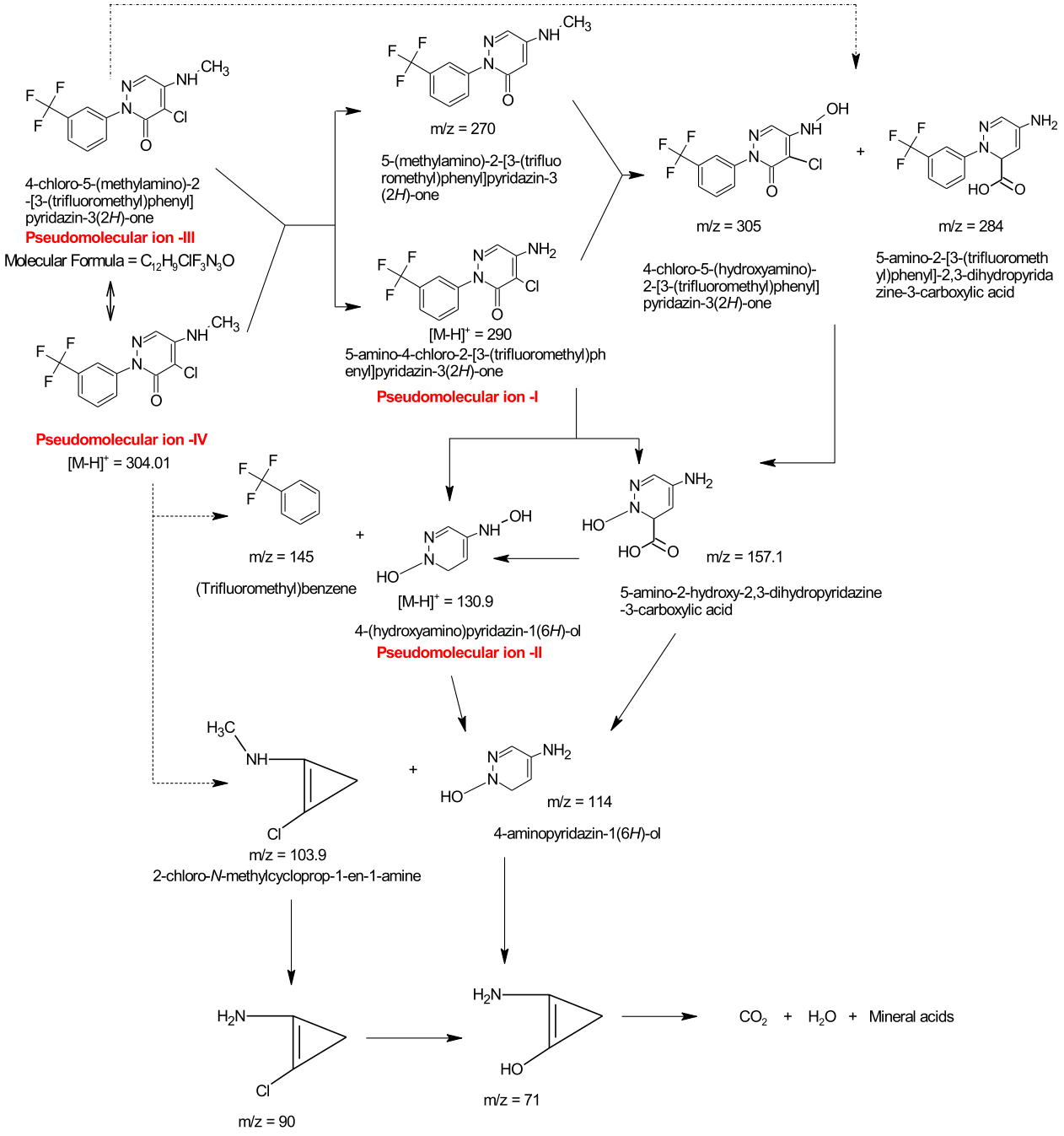

Scheme 1. Proposed mechanistic pathway for the mineralization of Norflurazon and its intermediates during sonophotocatalysis in the presence of Au–ZnO nanocatalysts.

Subsequently the enhanced rate of Norflurazon was achieved during the photocatalysis. When compared with the photocatalysis, the enhanced degradation attained during the sonocatalysis can be described as the sonoluminescence produced within the aqueous medium during the ultrasound irradiation significantly partake in the band gap excitation of Au–ZnO which enhances the production of effective radicals (Riaz and Ashraf, 2012; Ying and Williams, 1999). The rate constants observed for the sonophotocatalytic

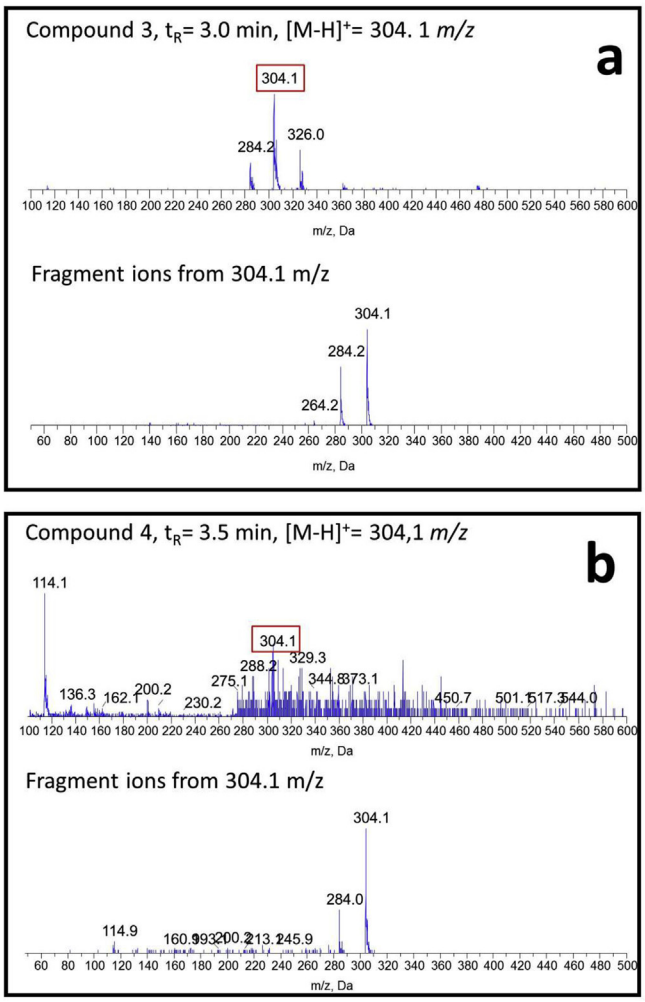

Fig. 10. HPLC-ESI-MS/MS chromatograms observed for the sonophotocatalytic mineralization of Norflurazon and its intermediates produced at (a) 240 min and (b) 300 min irradiation time.

degradation of Norflurazon at its optimized concentration in the presence of various nanocatalysts are shown in Table 1. The rate constant accomplished for the bare ZnO assisted sonophotocatalytic degradation is slightly greater than TiO_2. However the Au–ZnO augmented the sonophotocatalytic degradation when compared to the bare TiO_2 and ZnO.

The extended irradiation of Norflurazon was carried out for 5 h to evaluate the photocatalytic, sonocatalytic and sonophotocatalytic mineralization efficiency of Au–ZnO at its optimized concentrations (Fig. 8). The photolysis and sonolysis of Norflurazon could not make any significant changes in the initial concentration of Norflurazon after 5 h of irradiation. The order of mineralization was attained as follows sonophotocatalysis > sonocatalysis > photocatalysis which was the similar trend observed for the degradation process (Fig. 7). The sonophotocatalytic degradation of Norflurazon shown 58% of the total organic carbon (TOC) was removed from the initial concentration after 5 h of irradiation whereas the sonocatalytic and photocatalytic processes reached 43% and 17% of the TOC removal. The additive effect was achieved for the sonophotocatalytic mineralization due to the enhanced number of effective radicals being produced when compared with the individual advanced oxidation processes. Besides, the improved rate of mass transfer of Norflurazon to the nanocatalysts surface as well as the mass transfer of effective radicals from the nanocatalysts surface to the bulk solution lead to achieve the enhanced rate of mineralization during the sonophotocatalytic and sonocatalytic processes when compared with the photocatalytic mineralization.

The electro spray ionization-mass spectroscopy (ESI-MS) was employed to identify the intermediates produced during the sonophotocatalytic mineralization of Norflurazon. The aliquots were withdrawn at regular intervals for the ESI-MS analysis. The UHPLC-DAD-ESI MS/MS analysis shows the sonophotocatalytic mineralization of Norflurazon and the formation of four compounds which are detectable since 30 min of sonophotocatalytically irradiated Norflurazon and, numbered according to the retention time observed from the UHPLC chromatograms (Fig. 9; Table 2; compound I to IV). The first signal was identified as desmethyl Norflurazon (5-amino-4-chloro-2-[3-(trifluoromethyl) phenyl]pyridazin-3(2H)-one)), showing a pseudo molecular ion of $m/z = 290$ and a fragment of m/z 270.1. At retention time 2.3min, (4-(hydroxyamino) pyridazin-1(6H)-ol [Table 2; Scheme 1)] was detected with a pseudo molecular ion of m/z 130.9 and fragments of m/z 103.9, 90.0 and 81.0. The third signal (Fig. 10) corresponds to Norflurazon, and the last signal detected at 3.5 min could be assigned as Norflurazon isomer.

Ying and Williams (1999) reported the formation of Benzotrifluoride (m/z = 145; α,α,α-Trifluorotoluene) during the GC–MS analysis of the photodegradation of Norflurazon however, Benzotrifluoride is not detected during the ESI-MS analysis. In other words, the present experimental conditions cannot assist the identification of the Benzotrifluoride. The sonophotocatalytic irradiation greater than 300 min was expected to completely mineralize the Norflurazon and various intermediates produced during its degradation into CO_2, H_2O and other small molecular products. The tentative mechanism for the mineralization of Norflurazon is proposed in Scheme 1 which demonstrates the various pathways involved in the sonophotocatalytic decay of Norflurazon. The similar kind of decay pathway can be proposed for the photocatalytic and sonocatalytic degradation of Norflurazon. The identification of various intermediates was expected for the photocatalytic and sonocatalytic degradation apart from the intermediates observed for the sonophotocatalytic degradation.

4. Conclusion

A simple, convenient and one-step ultrasound assisted synthesis of gold and gold loaded ZnO nanocatalysts were demonstrated in the present study. The 42 kHz ultrasound persuaded the formation of gold nanoparticles and the appropriate distribution of gold nanoparticles on the surface of ZnO. The Au–ZnO nanocatalyst was showed 3.5 and 2.5 fold greater rate of mineralization of Norflurazon during the sonophotocatalysis and sonocatalysis when compared to the photocatalysis technique. The LCMS analysis of the sonophotocatalytically treated Norflurazon exhibits the formation of four pseudo molecular ions including the Norflurazon isomer. The further irradiation was expected to completely mineralize the Norflurazon into the CO_2, H_2O and mineral acids. The sonophotocatalysis exhibited in this study can be extended to study the degradation of wide spectrum of environmental contaminants and this developed methodology can be useful to study the mineralization of large quantity of Norflurazon.

Acknowledgments

The authors would like to thank FONDECYT Postdoctorado project No.: 3120095 and FONDECYT No.: 1130916 Government of Chile, Santiago, for financial assistance. The research work was financially supported by Council of Scientific and Industrial

Research (CSIR), New Delhi (CSIR Reference No. 02 (0021)/11/EMR-II).

References

Ahrens, W.H., 1994. Norflurazon. In: Herbicide Handbook, seventh ed. Weed Science Society of America, Champaign, IL, pp. 218–220.

Arias-Estevez, M., Lopez-Periago, E., Martinez-Carballo, E., Simal-Gandara, J., Mejuto, J., Garcia-Rio, L., 2008. The mobility and degradation of pesticides in soils and the pollution of groundwater resources. Agric. Ecosyst. Environ. 123, 247–260.

Bramley, P.M., 1993. Inhibition of carotenoid biosynthesis. In: Young, A., Britton, G. (Eds.), Carotenoids in Photosynthesis. Chapman and Hall, London, pp. 127–159.

Chen, Y., Zeng, D., Zhang, K., Lu, A., Wang, L., Peng, D., 2014. Au-ZnO hybrid nanoflowers, nanomultipods and nanopyramids: one pot reaction synthesis and photocatalytic properties. Nanoscale 6, 874–881.

Drogui, P., Lafrance, P., 2012. Pesticides and sustainable agriculture. In: Lichtfouse, E. (Ed.), Farming for Food and Water Security, 10. Springer, Netherlands, pp. 23–55.

Huang, J., Yin, Z., Zheng, Q., 2011. Applications of ZnO in organic and hybrid solar cells. Energy Environ. Sci. 4, 3861–3877.

Kamat, P.V., Meisel, D., 2002. Nanoparticles in advanced oxidation processes. Curr. Opin. Colloid Interface Sci. 7, 282–287.

Kim, J., Yong, K., 2012. A facile, coverage controlled deposition of Au nanoparticles on ZnO nanorods by sonochemical reaction for enhancement of photocatalytic activity. J. Nanopart. Res. 14, 1033 (1-10).

Lee, M.K., Kim, T.G., Kim, W., Sung, Y.M., 2008. Surface plasmon resonance (SPR) electron and energy transfer in noble metal-zinc oxide composite nanocrystals. J. Phys. Chem. C 112, 10079–10082.

Li, Y., Xie, W., Hu, X., Shen, G., Zhou, X., Xiang, Y., Zhao, X., Fang, P., 2010. Comparison of dye photodegradation and its coupling with light-to-electricity conversion over TiO2 and ZnO. Langmuir 26, 591–597.

Meng, Z., Zhu, L., Choi, J., Park, C.Y., Oh, W., 2012. Sonocatalytic degradation of Rhodamine B in the presence of C60and CdS coupled TiO_2 particles. Ultrason. Sonochem. 19, 143–150.

Mizukoshi, Y., Seino, S., Okitsu, K., Kinoshita, T., Otome, Y., Nakagawa, T., Yamamoto, T.A., 2005. Sonochemical preparation of composite nanoparticles of Au/c-Fe2O3 and magnetic separation of glutathione. Ultrason. Sonochem. 12, 191–195.

Morillo, E., Undabeytia, T., Cabrera, A., Villaverde, J., Maqueda, C., 2004. Effect of soil type on adsorption-desorption, mobility, and activity of the herbicide Norflurazon. J. Agric. Food Chem. 52, 884–890.

Ozgur, U., 2010. ZnO devices and applications: a review of current status and future prospects. Proc. IEEE 98, 1255–1268.

Pimentel, D., 1995. Amounts of pesticides reaching target pests: environmental impacts and ethics. J. Agric. Environ. Ethics 8, 17–29.

Riaz, U., Ashraf, S.M., 2012. Latent photocatalytic behavior of semi-conducting poly (1-naphthylamine) nanotubes in the degradation of Comassie Brilliant Blue RG-250. Sep. Purif. Technol. 95, 97–102.

Sakthivel, S., Neppolian, B., Shankar, M.V., Arabindoo, B., Palanichamy, M., Murugesan, V., 2003. Solar photocatalytic degradation of azo dye: comparison of photocatalytic efficiency of ZnO and TiO2. Sol. Energy Mater. Sol. Cells 77, 65–82.

Sathishkumar, P., Mangalaraja, R.V., Masilla, H.D., Gracia-Pinilla, M.A., Anandan, S., 2014. Appl. Catal. B: Environ. 160–161, 692–700.

Sathishkumar, P., Rubyraj, M., Anandan, S., Zhou, M., Ashokkumar, M., 2009. Visible light assisted photocatalytic degradation of acid red 88 using Au-ZnO nanophotocatalysts. Water Sci. Technol. 60, 1589–1596.

Subramanian, V., Wolf, E.E., Kamat, P.V., 2003. Green emission to probe photoinduced charging events in ZnO-Au nanoparticles. Charge distribution and fermi-level equilibration. J. Phys. Chem. B 107, 7479–7485.

Umar, A., Akhtar, M.S., Al-Hajry, A., Al-Assiri, M.S., Almehbad, N.Y., 2012. Hydrothermally grown ZnO nanoflowers for environmental remediation and clean energy applications. Mater. Res. Bull. 47, 2407–2414.

Wang, G.Y., Zhang, W.X., Lian, H.L., Jiang, D.Z., Wu, T.H., 2003. Effect of calcination temperatures and precipitant on the catalytic performance of Au/ZnO catalysts for CO oxidation at ambient temperature and in humid circumstances. Appl. Catal. A Gen. 239, 1–10.

Wang, X., Ding, Y., Summers, C.J., Wang, Z.L., 2004. Large-scale synthesis of six-nanometer-wide ZnO nanobelts. J. Phys. Chem. B 108, 8773–8777.

Wang, Y., Li, X., Lu, G., Quan, G., Chen, X., 2008. Highly oriented 1-D ZnO nanorod arrays on zinc foil: direct growth from substrate, optical properties and photocatalytic activities. J. Phys. Chem. C 112, 7332–7336.

Wei, M., Famouri, L., Carroll, L., Lee, Y., Famouri, Parviz, 2013. Rapid and efficient sonochemical formation of gold nanoparticles under ambient conditions using functional alkoxysilane. Ultrason. Sonochem. 20, 610–617.

Wilkinson, R.E., 1985. Carotenogenic inhibition by Norflurazon in wheat. Pestic. Biochem. Physiol. 23, 370–377.

Wilson, P.C., Boman, B.J., 2011. Characterization of selected organo-nitrogen herbicides in south florida canals: exposure and risk assessments. Sci. Total Environ. 412–413, 119–126.

Wood, A., Giersig, M., Mulvaney, P., 2001. Fermi level equilibration in quantum dot-metal nanojunctions. J. Phys. Chem. B105, 8810–8815.

Ying, G., Williams, B., 1999. Photodegradation of Norflurazon in water. Toxicol. Environ. Chem. 71, 261–269.

Zhu, X., Wu, H., Yuan, Z., Kong, J., Shenc, W., 2009. Multiphonon resonant Raman scattering in N-doped ZnO. J. Raman Spectrosc. 40, 2155–2161.